

Role for the nuclear receptor-binding SET domain protein 1 (NSD1) methyltransferase in coordinating lysine 36 methylation at histone 3 with RNA polymerase II function

Agda Karina Lucio-Eterovic^a, Melissa M. Singh^{a,1}, Jeffrey E. Gardner^a, Chendhore S. Veerappan^b, Judd C. Rice^b, and Phillip B. Carpenter^{a,2}

^aDepartment of Biochemistry and Molecular Biology, University of Texas Health Science Center, Houston, TX 77030; and ^bDepartment of Biochemistry and Molecular Biology, University of Southern California Keck School of Medicine, Los Angeles, CA 90033

Edited* by George R. Stark, Lerner Research Institute NE2, Cleveland, OH, and approved August 19, 2010 (received for review March 2, 2010)

The NSD (nuclear receptor-binding SET domain protein) family encodes methyltransferases that are important in multiple aspects of development and disease. Perturbations in NSD family members can lead to Sotos syndrome and Wolf-Hirschhorn syndrome as well as cancers such as acute myeloid leukemia. Previous studies have implicated NSD1 (KMT3B) in transcription and methylation of histone H3 at lysine 36 (H3-K36), but its molecular mechanism in these processes remains largely unknown. Here we describe an NSD1 regulatory network in human cells. We show that NSD1 binds near various promoter elements and regulates multiple genes that appear to have a concerted role in various processes, such as cell growth/cancer, keratin biology, and bone morphogenesis. In particular, we show that NSD1 binding is concentrated upstream of gene targets such as the bone morphogenetic protein 4 (*BMP4*) and zinc finger protein 36 C3H type-like 1 (*ZFP36L1/TPP*). NSD1 regulates the levels of the various forms of methylation at H3-K36 primarily, but not exclusively, within the promoter proximal region occupied by NSD1. At *BMP4* we find that this reduces the levels of RNAP II recruited to the promoter, suggesting a role for NSD1-dependent methylation in initiation. Interestingly, we also observe that the RNAP II molecules that lie within *BMP4* have inappropriate persistence of serine-5 phosphorylation and reduced levels of serine-2 phosphorylation within the C-terminal domain (CTD) of the large subunit of RNAP II. Our findings indicate that NSD1 regulates RNAP II recruitment to *BMP4*, and failure to do so leads to reduced gene expression and abrogated levels of H3K36Me and CTD phosphorylation.

elongation | initiation | C-terminal domain | histone code | ChIP on chip

NSD1 (nuclear receptor-binding SET domain protein 1 or KMT3B) belongs to a family of mammalian histone lysine methyltransferases (NSD1, NSD2/WHSC1, and NSD3/WHSC1L1) that are important in multiple aspects of development and disease (1–7). Human NSD1 is a large protein composed of 2,696 residues and contains several motifs in the C-terminal half that are undoubtedly critical for its proposed functions in signaling and chromatin regulation. This includes a catalytic lysine methyltransferase SET domain and four zinc-binding PHD fingers. NSD1 was originally discovered in a two-hybrid screen through its ability to bind to nuclear receptors such as retinoic acid (8). Mice deficient in *NSD1* exhibit an embryonic lethal phenotype due to apoptosis at E10.5 (9). Nearly 5% of all human acute myeloid leukemia (AML) patients harbor a translocation in the *NSD1* gene at chromosome 5 that encodes for a chimeric protein encompassing the FG-repeat domain of NUP98 fused to the carboxy-terminus of NSD1 (10). This fusion protein has been shown to promote *HOX* gene activation by antagonizing repressive chromatin structure in a manner that depends on the methyltransferase activity of the SET domain (10). Furthermore, translocations involving NSD1 have been found in breast cancer (7), and epigenetic inactivation of the *NSD1* promoter through CpG hypermethylation has been shown to be important in neuroblastomas and glioblastomas (3). Therefore, translocation-driven NSD1 fusion

proteins behave as oncogenes in AML, but inactivation of NSD1 in neuroblastomas behaves as a tumor suppressor (3). In addition to its role in development and cancer, *NSD1* is haploinsufficient in Sotos syndrome (11), a childhood overgrowth disease characterized by a broad set of phenotypes, including macrocephaly, advanced bone age, facial dysmorphism, learning disabilities, and seizures (12).

Histone side chains undergo a plethora of posttranslational modifications (PTMs) that formulate a “histone code” (13–15). Histone PTMs initiate signaling events by recruiting “reader” proteins or through inducing structural changes in chromatin (13). Lysine residues, including H3-K36, can exist in up to four different forms: nonmethylated (Me0) and the mono-, di-, and trimethylated forms (Me1, Me2, and Me3, respectively). Although NSD1 was originally shown to methylate histones on both H4-K20 and H3-K36 in vitro (9), more recent experiments suggest that the enzyme, as well as its related family members from humans, worms, and flies, is specific for H3-K36 (16–19). Importantly, Li et al. (18) used defined nucleosomal substrates chemically modified at histone H3 to contain the various methylated forms of lysine 36, and showed that human NSD1 is a dimethylase specific for H3-K36. In addition to histones, NSD1 has recently been shown to activate the p65 subunit of NF- κ B through both mono- and dimethylation of lysine residues K218 and K221, respectively (20).

The biological significance of the various forms of H3-K36Me is poorly understood. In worms and humans, H3-K36Me3 has been shown to link transcription with splicing (21–23). In flies, H3-K36Me3 functions in dosage compensation (24). In yeast, H3-K36Me2 and H3-K36Me3 have both been implicated in transcription elongation, and this appears to be coupled to histone acetylation through recruitment of the Rpd3S deacetylase complex (14, 25–31), which maintains hypoacetylated chromatin in the wake of RNAP II function and prevents cryptic initiation. Rpd3S preferentially binds H3-K36Me2 and H3-K36Me3, but not H3-K36Me1 (30), indicating that the various methylated forms of H3-K36 specify distinct biological signals. In *Arabidopsis*, the di- and trimethylated states mark actively transcribed chromatin (32), and the levels of H3-K36Me2 and H3-K36Me3 have been shown to peak near the 3' end of active chicken genes (33). In yeast, H3-K36Me3 correlates with transcriptional frequency, and H3-K36Me2 has been linked to the on/off states of transcription (14). In humans, there is a slight preference for H3-K36Me1 at active promoters, and this mark has also been

Author contributions: A.K.L.-E., M.M.S., and P.B.C. designed research; A.K.L.-E., M.M.S., and J.E.G. performed research; J.C.R. contributed new reagents/analytic tools; A.K.L.-E., C.S.V., J.C.R., and P.B.C. analyzed data; and A.K.L.-E. and P.B.C. wrote the paper.

The authors declare no conflict of interest.

*This Direct Submission article had a prearranged editor.

¹Present address: Department of Pediatrics Research, Children's Cancer Hospital at MD Anderson, University of Texas MD Anderson Cancer Center, Houston, TX 77030.

²To whom correspondence should be addressed. E-mail: phillip.b.carpenter@uth.tmc.edu.

This article contains supporting information online at www.pnas.org/lookup/suppl/doi:10.1073/pnas.1002653107/-DCSupplemental.

detected in transcriptionally active regions of the β -globin locus (34). At the human globin genes, H3-K36Me1 is broadly distributed, but the di- and trimethylation marks correlate with transcription in opposite ways (34).

Despite the fact that NSD1 targets H3-K36, little is known about its role in transcriptional regulation. To further delineate the role of NSD1 in transcription and chromatin regulation, we identified and validated an NSD1 transcriptional network in multiple human cell lines. We performed a chromatin immunoprecipitation/microarray (“ChIP on chip”) assay and determined a set of over 300 candidate target genes in HCT116 cells for NSD1. We found that NSD1 binds to the promoter regions of genes implicated in various processes, including those consistent with its known role in diseases such as cancer and Sotos. In particular, we show that NSD1 regulates transcription of bone morphogenetic protein 4 (*BMP4*). Here, NSD1 binding is concentrated in a region $\approx 1,200$ bp upstream ($-1,200$) of the *BMP4* promoter and enforces H3-K36Me levels within this region. Depletion of NSD1 reduces the levels of H3-K36Me1, 2, and 3, suggesting that NSD1 is a mono/dimethylase and that this modification serves as a potential substrate for trimethylation. A similar profile was found for *ZFP36L1/TPP*. We further show that in the absence of NSD1, the abrogated H3-K36Me levels at $-1,200$ reduces RNAP II occupancy at the *BMP4* promoter. We find that the RNAP II that does elongate through the *BMP4* gene is enriched in serine-5 phosphorylation and diminished in serine 2-phosphorylation. These data suggest that NSD1 is involved in the regulation of gene expression through stimulating the transition of RNAP II from an initiation to fully elongation-competent state.

Results

Predominant Expression of the Short Isoform of NSD1 in Multiple Cell Types. To begin to understand the role of NSD1 in chromatin regulation, we sought to determine the relative ratios of the short and long isoforms in various cell types. Through an examination of the *NSD1* gene on Ensembl, we deduced that the short isoform of NSD1 is differentiated from the long isoform by an inclusion of an additional 740 nucleotides that result from an intron-retention mechanism. In this particular case there is an mRNA splicing event that removes an intron from within exon 2 (Fig. 1A). This exon contains coding information that is part of the long form. To determine the extent of intron retention and hence the relative levels of the short and long isoforms of NSD1, we designed a PCR-based assay to differentiate between the long and short isoforms in various cell types. Using PCR conditions that could amplify both the long (939 bp) and short (199 bp) isoforms (with the same primer set), we reproducibly observed that the short isoform was predominantly expressed in a variety of cell types (Fig. 1B). Partial NSD1 clones were used as positive control for the short (exons 1–5) and long isoforms (exons 1–2).

Establishment of an NSD1 Transcriptional Network. Very little is known about the number and types of endogenous targets of NSD1. One study showed that NSD1 regulates *MEIS1* in cells of neuronal lineages (3). An earlier report showed that the *HOXA7*, 9, 10, and *MEIS1* genes are regulated by the NUP98-NSD1 oncoprotein that contains a fusion between Nup98 and the C-terminal half of NSD1 (10). However, it is not clear if NSD1 by itself or the fusion protein regulates these targets under “normal” conditions (10). To determine the natural genomic targets that NSD1 associates with, we first used homologous recombination (HR) to generate an epitope-tagged fusion at the 3' end of the endogenous *NSD1* gene on chromosome 5 in human colorectal cancer HCT116 cells (Fig. S1). Because the C terminus of NSD1 was previously shown to be dispensable for its methyltransferase activity and its interaction with the *HOX* locus (10), we were confident that manipulating the 3' end of *NSD1* would not interfere with the resulting activity of the protein in our subsequent analysis. Using this HCT116 NSD1-FLAG cell line, we performed a chromatin immunoprecipitation/microarray (ChIP on chip, or ChIP microarray) experiment with two-color tiling arrays.

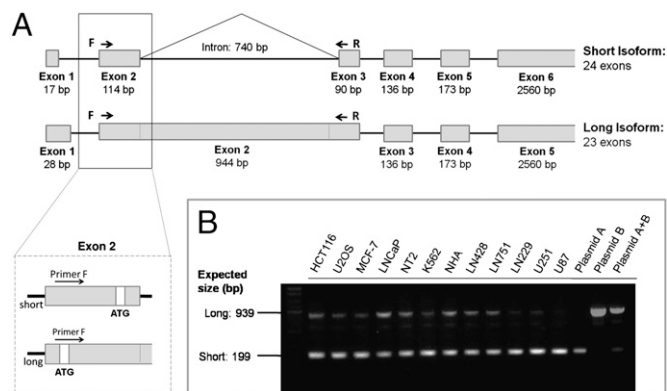


Fig. 1. Predominance of expression of the short NSD1 isoform in multiple cell types. (A) Intron-exon structure (not drawn to scale) of NSD1 gene. The diagrams show the intron retention mechanism that results in two isoforms. In detail: localization of the forward primer and ATG sites in exon 2 of both isoforms. (B) PCR analysis from cDNA using one primer set that recognizes sequences common to both isoforms of NSD1 in different cell lines: HCT116 (colorectal cancer cells), U2OS (osteosarcoma), MCF-7 (breast cancer), LNCaP (prostate cancer), NT-2 (teratocarcinoma), K562 (leukemia), NHA (normal human astrocytes), LN428, LN751, LN229, U251, U87 (glioblastomas). The PCR products were sequenced to confirm the amplification of the NSD1 short isoform. Sequences: primer F: TGATGCCGCCAGGATGGA and primer R: TGGCAATTCCTGTGAAGTAGATGATG. NSD1 partial clones for the short and long isoforms (plasmids A and B, respectively) were used as control [clone IDs 2117843 (A) and 3908832 (B); Open Biosystems].

HCT116 cells expressing NSD1-FLAG were subjected to a ChIP protocol with anti-FLAG antibodies (*Materials and Methods*). As NSD1 has been implicated in transcriptional events, we examined the ability of NSD1-FLAG to associate with any of 24,659 promoter regions throughout the human genome. Here, the promoter regions were covered by probes ranging from 50 to 75 bp in length with a median spacing of 50 bp. To identify significant peaks and to assign *P* values using a *t* test, we used the recently described MA2C algorithm that incorporates a normalization method based upon the GC content of the probes (35). Using *P* values ranging from 0.001 to 0.0005, we determined that there were over 300 candidate NSD1 targets in HCT116 cells. From this, we identified a spectrum of candidate targets for NSD1 in HCT116 cells (Table S1). This includes those genes implicated in cancer: Bone morphogenetic protein 4 (*BMP4*), Cathepsin D (*CTSD*), and Kruppel-like factor 6 (*KLF6*), von Hippel tumor suppressor (*VHL*), and Kallikreins *KLK6* and *KLK14*. Additionally, several cell cycle-related genes were identified: *CDK4*, *CDC6*, *CHEK1*, *CCNE1* (cyclin E), *CDKN2A*, and the cyclin B interacting protein *CCNB1IP1*. We found that NSD1 binds to the promoter regions of 20 different keratin genes, including two (*KRT3* and *KRT6B*) known to be regulated by the p65 subunit of NF- κ B. Moreover, we identified the p65 targets *SLC16A1*, *IGF2BP2* as candidate NSD1-regulated genes. We also identified the development and mental retardation candidate gene (*ZMYM3*) and the early response gene Tristetraprolin (*TTP* or *ZFP36L1*) that encodes an RNA binding protein as potential targets of NSD1 (36–39) (Table S1).

We used ChIP followed by real-time PCR (qPCR) to validate our ChIP microarray results. We confirmed the occupancy of NSD1 at multiple promoter elements, including *BMP4* (Fig. 2A). We chose to analyze the *BMP4* gene more thoroughly, because bone morphogenesis is perturbed in Sotos syndrome and because of the amenable size of the gene (7,100 bp). Because the microarrays contained probes that represented promoter regions, it remained possible that we would not have detected NSD1 binding events outside of this region. We therefore analyzed the distribution of NSD1 across the length of the entire *BMP4* gene in HCT116 cells. To examine this, we performed ChIP analysis

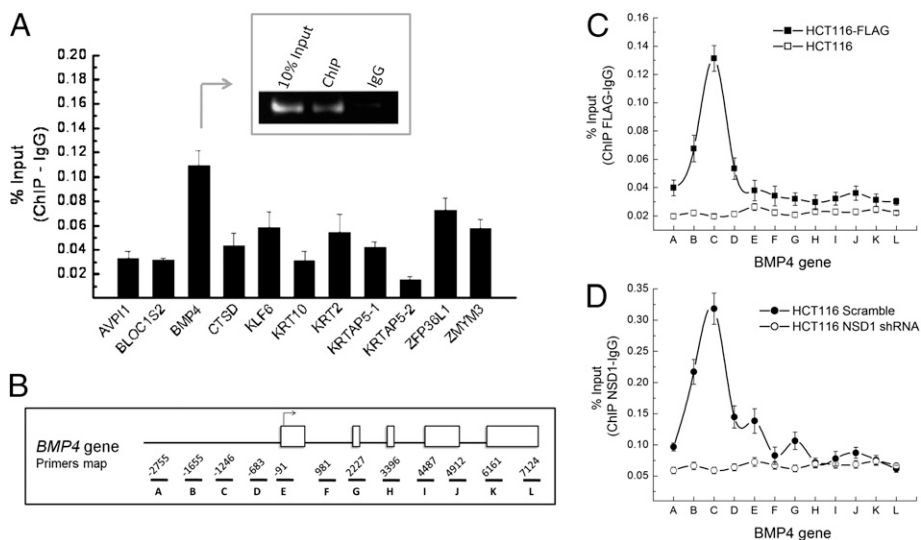


Fig. 2. (A) Validation of ChIP-on-chip data. Individual ChIP ($n = 4$) was performed for NSD1 targets in HCT116 NSD1-FLAG cells: *AVP11* (arginine vasopressin induced 1), *BLOC152* (biogenesis of lysosomal organelles complex1 subunit 2), *BMP4* (bone morphogenetic protein 4), *CTSD* (cathepsin D), *KLF6* (Kruppel-like factor 6), *KRT10* (keratin 10), *KRT2* (keratin 2), *KRTAP5-1* and 2 (keratin-associated protein 5: 1 and 2), *ZFP36L1* (zinc finger protein CH3-like), and *ZMYM3* (zinc finger MYM-type 3). Primer sequences are listed in Table S2. (Inset) ChIP at the *BMP4* promoter as a representative of the other individual ChIP experiments. (B) Diagram of *BMP4* intron/exon gene structure (not drawn to scale) showing the location of amplicons used to verify NSD1 binding profile. Numbers represent the first base of forward primer. Average sizes of amplicons are between 150 and 200 bp. Negative numbers indicate the region upstream +1 site (promoter region). Primer sequences are listed in Table S3. (C and D) NSD1 binding is concentrated upstream of the *BMP4* promoter (near $-1,200$). HCT116 NSD1-FLAG were processed for ChIP using FLAG (C) or NSD1 (D) antibodies. All primer sets were validated by DNA sequencing and through their ability to amplify one band. Control cells (parental cells void of the FLAG-tag and cells depleted of NSD1 by shRNA) were used with FLAG and NSD1 antibody, respectively, to show specificity of NSD1 binding by ChIP. Error bars in A, C, and D represent SD from the mean ($n = 3$).

with primer sets at multiple sites throughout the *BMP4* gene. Primers were designed covering the region from $-3,000$ bp to $7,100$ bp from the TSS site of *BMP4* gene (Fig. 2B). We found that NSD1 localization was concentrated to a region $1,200$ bp upstream of the $+1$ site of the *BMP4* promoter (Fig. 2C). Importantly, we failed to observe a ChIP signal in control HCT116 cells that did not harbor the FLAG-tagged allele, demonstrating the specificity for the interaction of NSD1 at the $-1,200$ region (Fig. 2C, open squares). We also confirmed this with an independent antibody specific to NSD1 (Fig. 2D). This second antibody gave slightly elevated NSD1 signals within the body of the gene but were absent in HCT116 cells depleted of NSD1 through shRNA (Fig. 2D, open circles). Therefore, the association between NSD1-FLAG and the $-1,200$ region of *BMP4* is conclusively a function of NSD1 and is not due to any possible FLAG-associated artifacts. Additionally, we performed an analogous set of experiments for the *ZFP36L1* gene and found that the binding profile of NSD1 to this target was also concentrated near 5' promoter elements (Fig. S2 A-C).

NSD1 Depletion Reduces Expression of Target Genes in a Cell Type-Specific Manner. To determine the impact of *NSD1* deficiency on target gene function, we used real-time PCR to measure the levels of candidate target gene expression in HCT116 cells depleted of NSD1 by shRNAs. For this, we generated two independent HCT116 cell lines where NSD1 was knocked down through the introduction of lentiviruses that express shRNAs targeting two independent sequences. A third line expressing a scrambled shRNA served as a control. Furthermore, to determine the generality of NSD1 regulation at candidate targets in additional cell types, we also generated U2OS osteosarcoma and MCF-7 breast cancer cells knocked down in NSD1 as well as their companion, scrambled controls. We found that knocking down *NSD1* resulted in severely reduced levels of NSD1 protein in all cell types examined (Fig. 3 Upper). Using real-time PCR, we found significant and reproducible reductions in transcript levels for several candidate targets, confirming that NSD1 regulates the expression of various targets identified in the ChIP

array (Fig. 3 Lower). Notably, we found that although the levels of the *KRT10* transcripts were severely reduced in MCF-7 cells defective in NSD1 function, *KRT10* levels were largely independent of NSD1 function in HCT116 cells. Moreover, *ZFP36L1/TPP* transcript levels were significantly abrogated in U2OS cells knocked down in NSD1, but they were only modestly affected in NSD1-deficient HCT116 cells. Therefore, NSD1 regulates target gene expression in a tissue-specific manner. Lentiviral shRNA1 was highly effective at knocking down NSD1 transcript and protein levels in HCT116 and U2OS cells (Fig. 3 A and B Upper). Although effective in these cell types, shRNA1 reduced *NSD1* transcript and protein levels by about a factor of 2 in MCF-7 cells (Fig. 3C). Interestingly, knockdown of NSD1 to these levels was nearly as effective in abrogating target gene expression to those levels seen in the highly effective shRNA2 (Fig. 3C). This finding is reminiscent of the fact that *NSD1* is haploinsufficient in Sotos syndrome and suggests that reduced, but not completely abolished, levels of *NSD1* transcription and translation are sufficient to creating a mutant state.

NSD1 Regulates H3-K36Me Levels at the *BMP4* Gene. Our *in vitro* assays with recombinant NSD1 show that the enzyme is specific for nucleosomal histone H3, but not octamers (Fig. S3). This is consistent with a recent report from Li et al. (18) that showed the specificity of NSD1 as a dimethylase (as well as NSD2 and NSD3) toward nucleosomal histone H3. To examine how NSD1 deficiency impacted histone methylation of H3-K36 at the *BMP4* locus *in vivo*, we performed ChIP assays with antibodies directed against the various methylated forms of H3-K36 or total H3 (as described in Materials and Methods). First, we confirmed the specificity of the antibodies in dot blots with various peptides containing the mono-, di-, and trimethylated forms of H3-K36 and several other histone methylated peptides (Fig. S4 A and B). Next, we examined the distribution of the various forms of H3-K36Me across the entire *BMP4* gene as a function of NSD1. When normalized to total H3, high levels of H3-K36Me1, 2, and 3 were reproducibly observed near $-1,200$ and coincided with the peak region of NSD1 binding, suggesting that NSD1 enforces methylation at H3-K36 within

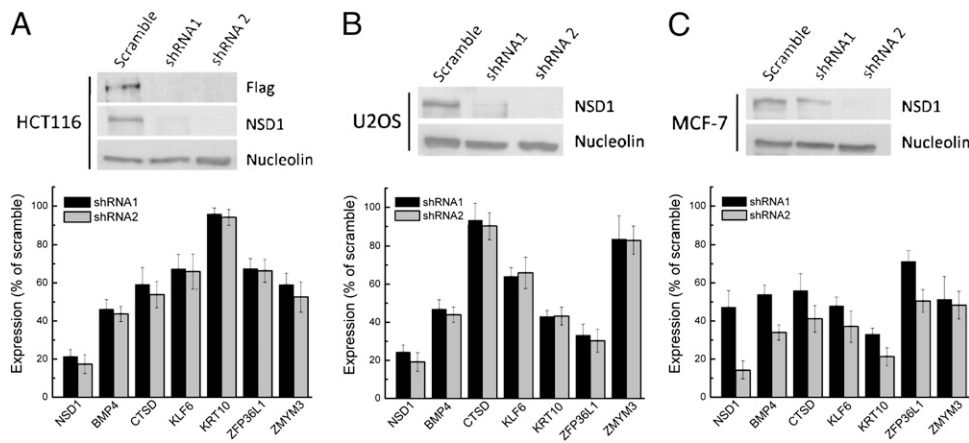


Fig. 3. Knockdown of NSD1 results in reduced expression of targets. Two different shRNAs against NSD1 or a scrambled control were transduced into HCT116 NSD1-FLAG, U2OS, and MCF-7 cells. (Upper) Immunoblotting shows efficacy of NSD1 knockdown in HCT116 (A), U2OS (B), and MCF-7 (C) cells. Nucleolin was used as loading control. (Lower) Real-time PCR for *NSD1*, *BMP4*, *CTSD*, *KLF6*, *KRT10*, *ZFP36L1*, and *ZMYM3* expression shows their levels of transcription in the absence of NSD1 in HCT116 ($n = 6$), U2OS ($n = 3$), and MCF-7 cells. Primers sequences are listed in Table S2. Error bars represent SD ($n = 3$).

this region. Indeed, we consistently detected reduced levels of all three forms of H3-K36Me at this region in NSD1 knockdown cells (Fig. 4 Left). Consistent with earlier studies that have determined that the levels of H3-K36Me2 and H3-K36Me3 peak near the 3' end of genes (33), we found that this trend is also phenocopied at *BMP4*. In particular, NSD1 knockdown cells generated reproducible reductions in the di- and trimethylation signals, but not to the same extent as what we found near $-1,200$ (Fig. 4 Left). Consistent with this, we also observed that NSD1 enforced H3-K36Me levels at *ZFP36L1* (Fig. S2 D and E).

NSD1 Regulates RNAP II Occupancy at the *BMP4* Promoter. Previous findings have linked H3-K36Me with gene activity, but the role of each modification and how it relates to RNAP II function is still unclear. Because NSD1 regulates the levels of H3-K36Me near $-1,200$, we examined the levels and distribution of RNAP II across the *BMP4* gene in the presence and absence of NSD1 function (Fig. 4 Right). Once recruited to promoter elements, the CTD is rapidly converted to hyperphosphorylated forms during the transition from transcriptional initiation to elongation (40). Here, RNAP II “escapes” the promoter region and transcribes along the length of the gene. Phosphorylation at S5 and S2 of the CTD is known to regulate the initiation and elongation properties of RNAP II, respectively. Serine 5 phosphorylation is present at the 5' end, but as the polymerase moves toward the 3' end, the serine-2 phosphorylated form predominates. Therefore, the status of serine-2 phosphorylation is indicative of elongation (41).

In HCT116 control cells (scramble shRNAs), we found that RNAP II levels consistently peaked near the +1 site (Fig. 4D). In contrast, in cells depleted of NSD1, we reproducibly observed reduced levels of RNAP II at the *BMP4* +1 site (Fig. 4D), suggesting that the lack of NSD1 caused a reduction in initiation. However, the total levels of RNAP II associated with *BMP4* chromatin downstream of the +1 site (i.e., nucleotides +3,396 to end) were not affected by the loss of NSD1 function (Fig. 4D). To explain this paradox, we hypothesized that the elongation efficiency of RNAP II was reduced in cells depleted of NSD1 in this region. In this scenario, RNAP II would be stalled at positions around amplicon +3,396, and a buildup of RNAP II at this locus would account for the equivalent levels of RNAP II detected in control and shRNA-treated cells. To examine the nature of elongating RNAP II at *BMP4* as a function of NSD1 activity, we determined the extent of phosphorylation at CTD serine residues 2 and 5 throughout *BMP4* (Fig. 4 E and F). Phosphospecific RNAP II antibodies were first validated by phosphatase treatment (Fig. S4C). In amplicons with equivalent amounts of total RNAP II (H-L), we found that the CTD possessed reduced levels of serine-2 phosphorylation (i.e., nearly a 70% reduction at +3,396), but slightly increased levels of serine-5 phosphorylation, a mark associated with initiation. This is accompanied by reduced levels of H3-K36Me3 at this locus. Such defects could account for the apparent stalling observed at *BMP4*. Because the levels of serine-2

and serine-5 phosphorylation increase and decrease, respectively, as the polymerase approaches the 3' end, our findings show that the absence of NSD1 generates RNAP II complexes that are defective in CTD phosphorylation.

Discussion

Defects in the NSD family cause various diseases, including Sotos syndrome and Wolf-Hirschhorn syndrome, as well as cancers such as AML, neuroblastomas, and glioblastomas. Despite the clinical importance of this family of enzymes, very little is known about their specific targets or mode of action. NSD2 has been shown to regulate cardiac transcription (42), but contradictory information has been reported in the literature with respect to its substrate specificity as well as that of other NSD family members (ref. 18 and references within). Despite such discrepancies, recent work with defined substrates has indicated that the catalytic SET domain of this family appears sensitive to the nature of its substrates (18). With respect to nucleosomal substrates, as opposed to octamers, our results show that NSD1 appears specific for H3-K36, a finding that is consistent with previous experiments from Li and coworkers (18). Additional experiments from Lu et al. (20) have shown that NSD1 is activated in response to cytokines and methylates nonnucleosomal targets such as the p65 subunit of NF- κ B. Here, NSD1 was shown to act as a mono- and dimethylase against lysine residues K218 and K221 of p65, respectively.

As NSD1 is an H3-K36-specific methyltransferase, we set out to define its targets in the context of transcription. Using a ChIP-on-chip strategy and a cell line engineered to express an endogenous epitope tag at the 3' end of the human *NSD1* gene, we identified a number of candidate NSD1 target genes in HCT116 cells. However, because we confirmed only a subset of the candidate NSD1 targets, we cannot formally exclude the possibility that some artifacts associated with the ChIP microarray procedure (i.e., cross-hybridization) may change the list of NSD1 targets. We also examined the role of NSD1 in the regulation of candidate targets in U2OS and MCF-7 cells. We found that the extent of NSD1-dependent regulation of its targets was cell-type specific as, for example, NSD1 regulation of the *ZFP36L1/TPP* gene was highest in U2OS cells but lowest in HCT116 cells. Because of this, and because NSD1 is activated in response to cytokines, it is likely that the NSD1 transcriptional network, including the extent of target gene regulation, will be variable and inducible in multiple cell types.

We found that the levels of *BMP4* were consistently reduced in all three examined cell types. We further examined the role of NSD1 in the regulation of *BMP4* transcription. Using FLAG antibodies with the NSD1-FLAG HCT116 cells (or control non-FLAG-tagged cells) as well as a second polyclonal antibody specific to NSD1, we reproducibly demonstrated that NSD1 associates primarily within a region $\approx 1,200$ bp upstream of the

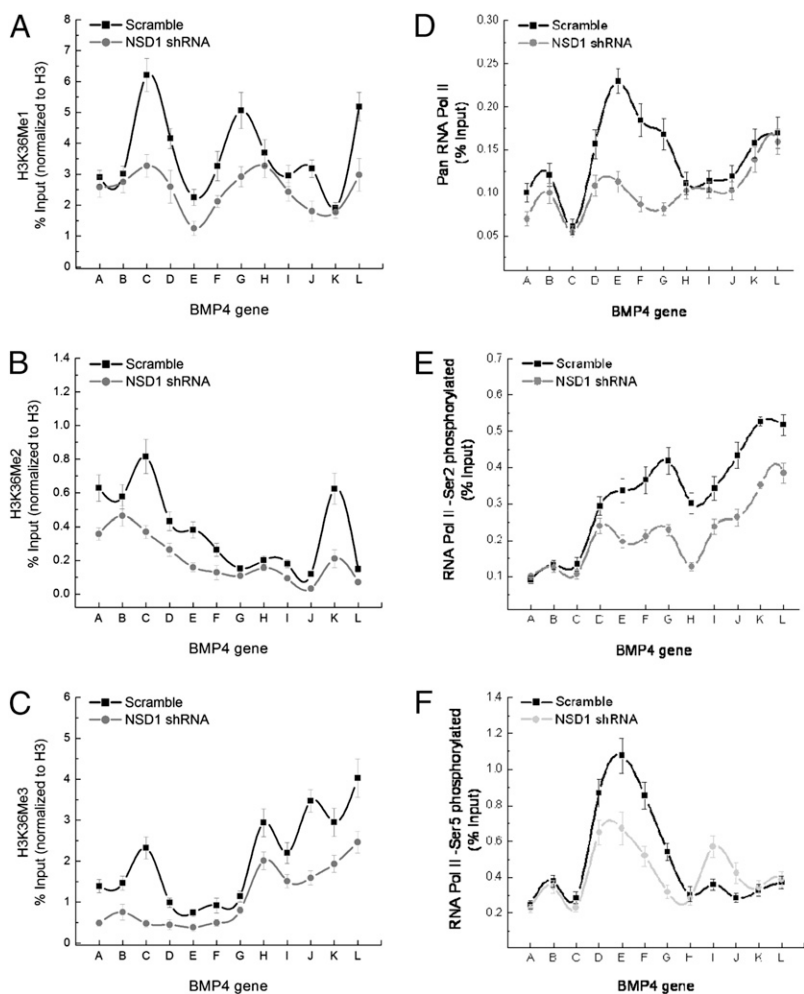


Fig. 4. (Left) H3K36 mono-, di-, and trimethylation profile at the *BMP4* locus in the presence or absence of NSD1. The levels of mono (A), di (B), and tri (C) H3-K36 methylation were measured by ChIP using specific antibodies in HCT116 cells, followed by real-time PCR. ChIP-specific signal (% input) was calculated using IgG as control as specified in *Materials and Methods*. The % input values were normalized to total H3 (% input H3K36Me/ $\%$ input unmodified H3). As the values were normalized by H3 values <1 may be expected. Error bars represent SD from the mean ($n = 3$). (Right) RNA polymerase II binding profile in the *BMP4* gene in the presence or absence of NSD1 function. Levels of pan (D), Ser-2-phosphorylated (E), and Ser-5-phosphorylated (F) forms of RNA Pol II were measured by ChIP using antibodies specific for RNA Pol II and its phosphorylated forms (Bethyl Laboratories) in HCT116 cells, followed by real-time PCR. ChIP specific signal (% input) was calculated using IgG as control, as specified in *Materials and Methods*. Error bars represent SD from the mean ($n = 3$). Primers (A-L) were designed along *BMP4* gene according to the diagram in Fig. 2B: -2,755 (A), -1,655 (B), -1,246 (C), -683 (D), -91 (E), 981 (F), 2,227 (G), 3,386 (H), 4,487 (I), 4,912 (J), 6,161 (K), and 7,124 (L).

BMP4 start site. In contrast, relative NSD1 levels were largely reduced within the body of the gene. A similar NSD1 binding profile was observed for the *ZFP36L1* target, suggesting that the localization of NSD1 to 5' elements is a general, but not necessarily exclusive, feature of the molecule.

We found that depletion of NSD1 abrogated the levels of H3-K36Me1, 2, and 3 at $-1,200$ and within the *BMP4* gene, indicating that NSD1 enforces an activating H3-K36Me signal at the *BMP4* locus. This was most pronounced at $-1,200$ and was accompanied by reduced levels of total RNAP II near $+1$. This is consistent with a role for H3-K36Me at $-1,200$ of *BMP4* in an initiation event and is interesting because most results have implicated H3-K36Me in elongation (24, 28). Therefore, those reader proteins specific for $-1,200$ of *BMP4* might be expected to be different from RpdS3, a complex that binds to H3-K36Me during elongation (28). Our data raises the question of how NSD1, located primarily near $-1,200$, can influence downstream H3-K36 methylation events. Because NSD1 occupancy is largely reduced inside the *BMP4* gene, we suggest that NSD1 directly methylates nucleosomes around the $-1,200$ region, but indirectly influences H3-K36Me levels far downstream of the *BMP4* start site. In this scenario, reduced and/or faulty initiation events due to NSD1 deficiency could indirectly alter elongation efficiency. Those RNA Pol II molecules that elongate in the context of NSD1 deficiency would be expected to show alterations in CTD phosphorylation (Fig. 5 B and C) that would be expected to be accompanied by defects in those H3-K36Me events that are catalyzed in a cotranscriptional manner.

We advocate a model where NSD1 deposits mono- and/or dimethyl groups onto H3-K36, and that these serve as potential

substrates for the trimethylase. As we observe, in the absence of NSD1, the levels of all three forms of H3-K36Me are affected, but determining which form(s) are responsible for recruiting RNAP II to promoters will require further experimentation. However, such a function of NSD1 may not be conserved by other NSD family members. For example, knockdown of the NSD2 methyltransferase in HeLa cells led to reduced levels of H3-K36Me2, but not of H3-K36Me1 or H3-K36Me3 (18). Though informative, it is important to note that this study analyzed global H3-K36Me2 and 3 levels and was not conducted at the resolution of an individual target gene. Our knockdown cells show little, if any, differences in global levels of H3-K36Me. Moreover, a conflicting result identified NSD2 as an H3-K36 specific trimethylase in vivo that represses cardiac-specific transcription (42). This finding is curious in light of reports describing the role of HYPB/SET2 as the only H3-K36-specific trimethylase in murine and fly cells (43). We found no evidence for a repressive role of NSD1 at its gene targets in the three cell types examined here. Despite this, NSD1 has also been described to repress *MEIS1* in neuroblastoma cells (3) as well as in reporter assays through its interaction with the NIZP1 zinc finger protein (44). We did not find that *MEIS1* was expressed in our cells. Therefore, NSD1, and by extension its other family members, likely performs tissue-specific roles in chromatin function.

We routinely observed that RNAP II levels peaked at the $+1$ site of the *BMP4* promoter. As abrogation of H3-K36Me at $-1,200$ resulted in a reduction in RNAP II occupancy at $+1$ of the *BMP4* promoter, optimal RNAP II promoter occupancy depends on the status of NSD1-dependent methylation at $-1,200$. By itself, RNAP II cannot accurately recognize promoters to initiate transcription

(45). Rather, transcriptional activators and/or chromatin modifiers can increase transcription initiation by improving the efficiency of RNAP II loading onto promoters. Our data suggest that the NSD1-dependent methyltransferase activity concentrated near $-1,200$ promotes RNAP II recruitment to the $+1$ site. This indicates that NSD1 functions in initiation at *BMP4* by acting as a transcriptional coactivator in HCT116 cells through maintaining the levels of H3-K36Me at this region. Although we failed to detect immunoprecipitates indicative of physical interactions between RNAP II and NSD1, we speculate that the $-1,200$ region could be in physical contact with the $+1$ site through bridging factors. Here, NSD1-dependent methyl marks could recruit effectors (i.e., acetylases) to provide RNAP II with access to the promoter. Whether the decreased levels of RNAP II observed in NSD1-deficient cells reflects the lack of recruitment of factors known to be required for RNAP II-dependent initiation (i.e., TFIIB, D, E, F, and H) remains to be determined. In summary, our data link NSD1 activity with RNAP II loading through H3-K36Me, and suggests that this could, at least indirectly, impact elongation. How NSD1 operates in initiation (i.e., promoter escape and pausing) and what the role of the individual methylation marks are in this process remains the subject of future studies.

Materials and Methods

Cell Lines, Reagents, and Treatment. Cell lines used in this study were obtained from American Type Culture Collection (ATCC). Cells were cultured in DMEM containing 10% FBS, and maintained in a humidified incubator (5% CO₂) at 37 °C. To detect FLAG signal on Western blotting or in ChIP experiments we used FLAG M2 (Sigma) as per recommendation of the manufacturer. H3 antibody was obtained from Abcam (ab1791); H3K36Me1, Me2, and Me3 antibodies were purchased from Abcam (9048), Upstate (369), and Abcam (9050), respectively. An NSD1-specific antibody was obtained from Bethyl Laboratories (BL715). RNA polymerase II antibodies (pan, Ser2-P, and Ser5-P) were also purchased from Bethyl Laboratories as AbVantage Pack (A310-190A). Additional experimental details are described in *SI Materials and Methods*.

ACKNOWLEDGMENTS. We thank Dr. Pierre Chambon (Strasbourg, France) for the gift of the murine NSD1 cDNA; Dr. Z. Wang (Case Western, Cleveland, OH) for plasmids and protocols for generating FLAG knockin cells; Dr. Joseph Alcorn (University of Texas, Houston, TX) for adenoviruses; and Dr. Shelley Barton (University of Texas-M. D. Anderson Cancer Center, Houston, TX) and Dr. Eric Wagner (University of Texas, Houston, TX) for other reagents. J.C.R. is a Pew Scholar in the Biomedical Sciences and is partially supported by National Institutes of Health Grant GM075094. This work was supported by Welch Foundation Grant AU-1569 (to P.B.C.) and National Institutes of Health Grant R56GM065812 (to P.B.C.).

- Angrand PO, et al. (2001) NSD3, a new SET domain-containing gene, maps to 8p12 and is amplified in human breast cancer cell lines. *Genomics* 74:79–88.
- Battaglia A, Filippi T, Carey JC (2008) Update on the clinical features and natural history of Wolf–Hirschhorn (4p-) syndrome: Experience with 87 patients and recommendations for routine health supervision. *Am J Med Genet C Semin Med Genet* 148C:246–251.
- Berdasco M, et al. (2009) Epigenetic inactivation of the Sotos overgrowth syndrome gene histone methyltransferase NSD1 in human neuroblastoma and glioma. *Proc Natl Acad Sci USA* 106:21830–21835.
- Bergemann AD, Cole F, Hirschhorn K (2005) The etiology of Wolf–Hirschhorn syndrome. *Trends Genet* 21:188–195.
- Keats JJ, et al. (2005) Overexpression of transcripts originating from the MMSET locus characterizes all t(4;14)(p16;q32)-positive multiple myeloma patients. *Blood* 105:4060–4069.
- Stec I, et al. (1998) WHSC1, a 90 kb SET domain-containing gene, expressed in early development and homologous to a Drosophila dysmorphia gene maps in the Wolf–Hirschhorn syndrome critical region and is fused to IgH in t(4;14) multiple myeloma. *Hum Mol Genet* 7:1071–1082.
- Zhao Q, et al. (2009) Transcriptome-guided characterization of genomic rearrangements in a breast cancer cell line. *Proc Natl Acad Sci USA* 106:1886–1891.
- Huang N, et al. (1998) Two distinct nuclear receptor interaction domains in NSD1, a novel SET protein that exhibits characteristics of both corepressors and coactivators. *EMBO J* 17:3398–3412.
- Rayasam GV, et al. (2003) NSD1 is essential for early post-implantation development and has a catalytically active SET domain. *EMBO J* 22:3153–3163.
- Wang GG, Cai L, Pasillas MP, Kamps MP (2007) NUP98-NSD1 links H3K36 methylation to Hox-A gene activation and leukaemogenesis. *Nat Cell Biol* 9:804–812.
- Kurotaki N, et al. (2002) Haploinsufficiency of NSD1 causes Sotos syndrome. *Nat Genet* 30:365–366.
- Leventopoulos G, et al. (2009) A clinical study of Sotos syndrome patients with review of the literature. *Pediatr Neurol* 40:357–364.
- Jenuwein T, Allis CD (2001) Translating the histone code. *Science* 293:1074–1080.
- Shilatifard A (2006) Chromatin modifications by methylation and ubiquitination: implications in the regulation of gene expression. *Annu Rev Biochem* 75:243–269.
- Turner BM (2002) Cellular memory and the histone code. *Cell* 111:285–291.
- Bell O, et al. (2007) Localized H3K36 methylation states define histone H4K16 acetylation during transcriptional elongation in Drosophila. *EMBO J* 26:4974–4984.
- Bender LB, et al. (2006) ME5-4: An autosome-associated histone methyltransferase that participates in silencing the X chromosomes in the *C. elegans* germ line. *Development* 133:3907–3917.
- Li Y, et al. (2009) The target of the NSD family of histone lysine methyltransferases depends on the nature of the substrate. *J Biol Chem* 284:34283–34295.
- Stabell M, Larsson J, Aalen RB, Lambertsson A (2007) Drosophila dSet2 functions in H3-K36 methylation and is required for development. *Biochem Biophys Res Commun* 359:784–789.
- Lu T, et al. (2010) Regulation of NF-kappaB by NSD1/FBXL1-dependent reversible lysine methylation of p65. *Proc Natl Acad Sci USA* 107:46–51.
- Kolasinska-Zwiercz P, et al. (2009) Differential chromatin marking of introns and expressed exons by H3K36me3. *Nat Genet* 41:376–381.
- Sims RJ, 3rd, Reinberg D (2009) Processing the H3K36me3 signature. *Nat Genet* 41:270–271.
- Spies N, Nielsen CB, Padgett RA, Burge CB (2009) Biased chromatin signatures around polyadenylation sites and exons. *Mol Cell* 36:245–254.
- Larschan E, et al. (2007) MSL complex is attracted to genes marked by H3K36 trimethylation using a sequence-independent mechanism. *Mol Cell* 28:121–133.
- Carrozza MJ, et al. (2005) Histone H3 methylation by Set2 directs deacetylation of coding regions by Rpd35 to suppress spurious intragenic transcription. *Cell* 123:581–592.
- Joshi AA, Struhl K (2005) Eaf3 chromodomain interaction with methylated H3-K36 links histone deacetylation to Pol II elongation. *Mol Cell* 20:971–978.
- Kaplan CD, Laprade L, Winston F (2003) Transcription elongation factors repress transcription initiation from cryptic sites. *Science* 301:1096–1099.
- Kizer KO, et al. (2005) A novel domain in Set2 mediates RNA polymerase II interaction and couples histone H3 K36 methylation with transcript elongation. *Mol Cell Biol* 25:3305–3316.
- Lee JS, Shilatifard A (2007) A site to remember: H3K36 methylation a mark for histone deacetylation. *Mutat Res* 618:130–134.
- Li B, et al. (2009) Histone H3 lysine 36 dimethylation (H3K36me2) is sufficient to recruit the Rpd3s histone deacetylase complex and to repress spurious transcription. *J Biol Chem* 284:7970–7976.
- Morris SA, et al. (2005) Histone H3 K36 methylation is associated with transcription elongation in Schizosaccharomyces pombe. *Eukaryot Cell* 4:1446–1454.
- Xu L, et al. (2008) Di- and tri- but not monomethylation on histone H3 lysine 36 marks active transcription of genes involved in flowering time regulation and other processes in Arabidopsis thaliana. *Mol Cell Biol* 28:1348–1360.
- Bannister AJ, et al. (2005) Spatial distribution of di- and tri-methyl lysine 36 of histone H3 at active genes. *J Biol Chem* 280:17732–17736.
- Kim A, Kiefer CM, Dean A (2007) Distinctive signatures of histone methylation in transcribed coding and noncoding human beta-globin sequences. *Mol Cell Biol* 27:1271–1279.
- Song JS, et al. (2007) Model-based analysis of two-color arrays (MA2C). *Genome Biol* 8:R178.
- Bell SE, et al. (2006) The RNA binding protein Zfp3611 is required for normal vascularisation and post-transcriptionally regulates VEGF expression. *Dev Dyn* 235:3144–3155.
- Chen D, Zhao M, Mundy GR (2004) Bone morphogenetic proteins. *Growth Factors* 22:233–241.
- Simmen RC, et al. (2010) The emerging role of Krüppel-like factors in endocrine-responsive cancers of female reproductive tissues. *J Endocrinol* 204:223–231.
- van der Maarel SM, et al. (1996) Cloning and characterization of DXS6673E, a candidate gene for X-linked mental retardation in Xq13.1. *Hum Mol Genet* 5:887–897.
- Komarnitsky P, Cho EJ, Buratowski S (2000) Different phosphorylated forms of RNA polymerase II and associated mRNA processing factors during transcription. *Genes Dev* 14:2452–2460.
- Buratowski S (2009) Progression through the RNA polymerase II CTD cycle. *Mol Cell* 36:541–546.
- Nimura K, et al. (2009) A histone H3 lysine 36 trimethyltransferase links Nkx2-5 to Wolf–Hirschhorn syndrome. *Nature* 460:287–291.
- Edmunds JW, Mahadevan LC, Clayton AL (2008) Dynamic histone H3 methylation during gene induction: HYPB/Set2 mediates all H3K36 trimethylation. *EMBO J* 27:406–420.
- Nielsen AL, et al. (2004) Nizp1, a novel multitype zinc finger protein that interacts with the NSD1 histone lysine methyltransferase through a unique C2HR motif. *Mol Cell Biol* 24:5184–5196.
- Ptashne M, Gann A (1997) Transcriptional activation by recruitment. *Nature* 386:569–577.

Supporting Information

Lucio-Eterovic et al. 10.1073/pnas.1002653107

SI Materials and Methods

Generation of Endogenous FLAG-Tagged NSD1. DNA encoding the 3xFLAG epitope tag was introduced by homologous recombination into the endogenous *NSD1* locus using a protocol recently described by Zhang et al. (1). A targeting vector containing sequences homologous to the 5' and 3' regions flanking the stop codon of the *NSD1* gene (left and right arm primers) was constructed and packaged into the adeno-associated virus (rAAV). HCT116 cells were infected with the virus and selected for neomycin-resistant clones. Clones containing correct integration of the targeting construct were identified by genomic PCR (screening primers; see below). In cells containing the targeting vector, a PCR product was detected using primers that are complementary to the neomycin cassette and upstream or downstream of the *NSD1* sequences used for the targeting vector; the parental HCT116 cells did not produce a product. We deleted the neomycin gene from targeted clones using an adenovirus expressing Cre recombinase. Individual colonies were verified for loss of the neomycin cassette by PCR (Cre screening primers; see below). Excision of the neomycin gene results in a 225-bp product corresponding to the wild-type allele and a ~500-bp product for the tagged allele. Colonies that were positive for loss of the neomycin cassette were pooled and analyzed for the presence of epitope-tagged protein that was detectable in nuclear extracts using M2-FLAG antibodies. Primers used include primer set 1: (left arm) F_GGGAAAGTAATCCCAATCCTTGGTTTCC; R_GGAGACATGCCTTCTGTTCTGATTCTG CACTTGTG; primer set 2: F_GGTCCCATTACCAATCAATGTACATGAACAAC; R_GGCATAGTCAGAGCCTTCCAGAGATGCC; Screening: (left arm) F_GTGAGCAGGACAGTGTGA; R_GTTGTGCCAGTCATAGCCG; (right arm) F_TCTGGATTTCATCGACTGTGG; R_CTC-TAAACACCACCCTCTTGCC; and primer set 3: F_TCTTA-ACCAGGCTCCTTCCA; R_CCCACTGGCTAATGTCACAA.

Chromatin Immunoprecipitation Assays (ChIP). The ChIP-promoter microarray hybridization analysis was performed by NimbleGen Systems Inc. Sample preparation was performed as follows. HCT116 cells expressing NSD1-FLAG were cross-linked in 1.0% formaldehyde followed by resuspension in L1 lysis buffer [50 mM Hepes KOH (pH 7.5), 140 mM NaCl, 1 mM EDTA, 10% glycerol, 0.5% Nonidet P-40, 0.25% Triton X-100]. Cells were then washed and sonicated eight times for 20 s. The sonicated chromatin was used for immunoprecipitation (IP) with M2 FLAG antibody (Sigma) complexed to Dynabeads in a rotating platform at 4 °C overnight. The beads were then washed eight times in RIPA buffer. Washed beads were incubated with elution buffer [10 mM Tris (pH 8.0), 1 mM EDTA, 1% SDS] for 10 min at 65 °C. After centrifugation, the supernatant was incubated at 65 °C overnight to reverse the cross-linking reaction. The DNA was isolated and amplified with a Sigma WGA kit following the manufacturer's protocol and submitted to NimbleGen's ChIP-chip microarray services. The data were initially analyzed by NimbleGen's Signal Map software. Individual, targeted ChIP experiments were carried out as previously described (2). Briefly, cells were cross-linked in formaldehyde followed by lysis in IP buffer with protease inhibitors [150 mM NaCl, 50 mM Tris-HCl (pH 7.5), 5 mM EDTA, 0.5% Nonidet P-40, 1% Triton X-100]. After centrifugation, the nuclear pellet was washed with IP buffer and sonication was performed (fifteen 1-s-long pulses with 2 min on ice between cycles). Sheared chromatin equivalent to 2 million cells was used for ChIP. Ten percent of this was used as a control for

the amount of input DNA used in precipitations. After pre-clearing the chromatin with protein A/G agarose beads, samples were incubated with specific antibodies or nonspecific IgG antibody for 4 h at 4 °C. Protein A/G agarose beads washed in IP buffer were then added to the antibody-chromatin samples, and the mixture was rotated at 4 °C for an additional hour. The IPs were then sequentially washed in low- and high-salt buffers (low = buffer D with 150 mM NaCl; high = buffer D with 500 mM NaCl) followed by a LiCl wash [0.25 mM LiCl, 1.0% Nonidet P-40, 1.0% deoxycholate, 1.0 mM EDTA, 10 mM Tris (pH 8.0)] and finally two washes with TE [1.0 mM EDTA, 10 mM Tris (pH 8.0)]. DNA was isolated from the beads using chelex (10%) beads followed by boiling (10 min) and subsequent treatment with proteinase K (20 µg) for 30 min. The resulting DNA was used as a template for real-time PCR reactions. Data obtained by real-time PCR for each specific antibody were normalized to IgG control and plotted as percent input (% input ChIP – % input IgG). Input samples (unprecipitated chromatin) from each condition were serially diluted and used as a standard for the PCR reactions to allow comparison among different primer sets. All of the shown data represents the average of at least three independent ChIP experiments.

Real-Time PCR. Gene expression was determined by real-time PCR (qPCR). Total cellular RNA was extracted using Qiagen RNeasy Mini Kit (Qiagen) and RNA was reverse-transcribed to single-stranded cDNA using the High Capacity cDNA Reverse Transcription Kit (Applied Biosystems) according to the manufacturer's protocol. RNA samples were treated with DNase with a DNA-free kit (Ambion) to avoid the presence of genomic DNA in our preparations. mRNA expression levels were evaluated using an Mx3000 Stratagene qPCR instrument (Stratagene). Amplifications were obtained using SYBR green (Quanta) or TaqMan probes (Applied Biosystems). Blank and negative controls (no reverse transcriptase) were performed in parallel to verify amplification efficiency within each experiment. To normalize for differences in the amount of total cDNA added to each reaction, glyceraldehyde-3-phosphate dehydrogenase (GAPDH) gene expression was used as an endogenous control. To obtain the Ct (cycle) values, we established a threshold of 2. All reactions were performed in duplicate, and all procedures were carried out at 4 °C. The extent of change in expression of each gene was calculated using the delta-Ct (Δ Ct) method. All primer sets used to generate PCR products were sequenced to check for amplification of the correct target. The primer sequences are listed in Table S2. The catalog numbers for Taqman probes from Applied Biosystems are: NSD1 (Hs01076927), BMP4 (Hs00370076), and GAPDH (4352934E).

Western Blotting. For protein analysis by Western blotting, 30 µg of nuclear protein for each sample was loaded and separated by SDS/PAGE. Proteins were transferred to PVDF membranes, and the membranes were blocked in 5.0% BSA. The primary antibodies were diluted in TBS with Tween-20 (TBST) containing 5.0% BSA, and the membranes were incubated for 1 h at room temperature. The membranes were then washed three times with TBST, incubated with the respective secondary antibody, and washed again three times with TBST. The secondary antibody was visualized using the electron chemiluminescent reagent (Pierce).

shRNA-Targeted Protein Knockdown. pLKO.1-puro lentiviral vectors expressing nontarget control shRNA (SHC002, or "scram-

ble”) or two different NSD1-specific shRNAs [lentiviral particles: TRCN0000061356 (shRNA 1) and TRCN0000061371 (shRNA 2)] were purchased from Sigma–Aldrich. The sequences of each shRNA were GCAGCCAAGATGCAGTGTAAA (shRNA 1) and TCCAGTGAGAACTCGTTAATA (shRNA 2), respectively. Lentiviral particles carrying each shRNA were added twice (24 and 48 h) to the cells in a ratio of 13:1 in the presence of polybrene. After puromycin selection, the cells were assayed for knockdown efficiency by real-time PCR and Western blotting as described.

Histone Methyltransferase (HMTase) Assays. We optimized expression of a pCDNA3.1 vector containing an N-terminal hemagglutinin (HA)-tagged NSD1 construct with residues 1–267 removed (HA-mNSD1). As a negative control, we generated a catalytically inactive version of HA-mNSD1 (HA-mNSD1-mut) by introducing a double-point mutant in the SET domain (N2020A, H2021A). These constructs were expressed in 293T cells and isolated by immunoprecipitation with mouse HA-probe antibody and Protein A/G PLUS agarose (Santa Cruz). The beads were

washed twice with TBS [50 mM Tris-HCl (pH 7.5), 150 mM NaCl] and 0.05% Nonidet P-40, twice with TBS, and then equilibrated in HMTase buffer [50 mM Tris-HCl (pH 8.5), 5 mM MgCl₂]. Histone octamers and mononucleosomes were prepared as described previously by Luger et al. (3). Octamers were reconstituted from HeLa core histones by dialysis and purified on a Sephacryl S-200 gel filtration column. Mononucleosomes were reconstituted by salt dialysis using the 277-bp “601” nucleosome stabilizing sequence from pGEM3z-601. HMTase reactions were carried out in a 25- μ L reaction volume containing 12 μ g of histone octamers or mononucleosomes in HMTase buffer with 0.2 mM DTT and 20 μ M S-adenosyl methionine (SAM), and 1 μ L 3H-methyl SAM (>50 Ci/mmol; MP Biomedical) for 3 h at 30 °C. Each reaction contained 5.0 μ L of agarose beads with either the HA-mNSD1 or HA-mNSD1-mut immunoprecipitate. The reactions were stopped with SDS sample buffer and separated on a 4–20% Precise Protein gradient gel (Pierce). The proteins were transferred to a PVDF membrane, Ponceau stained, treated with EN³HANCE spray (Perkin-Elmer) and analyzed by fluorography.

1. Zhang X, et al. (2008) Epitope tagging of endogenous proteins for genome-wide ChIP-chip studies. *Nat Methods* 5:163–165.
2. Nelson JD, Denisenko O, Bomsztyk K (2006) Protocol for the fast chromatin immunoprecipitation (ChIP) method. *Nat Protoc* 1:179–185.

3. Luger K, Rechsteiner TJ, Richmond TJ (1999) Expression and purification of recombinant histones and nucleosome reconstitution. *Methods Mol Biol* 119:1–16.

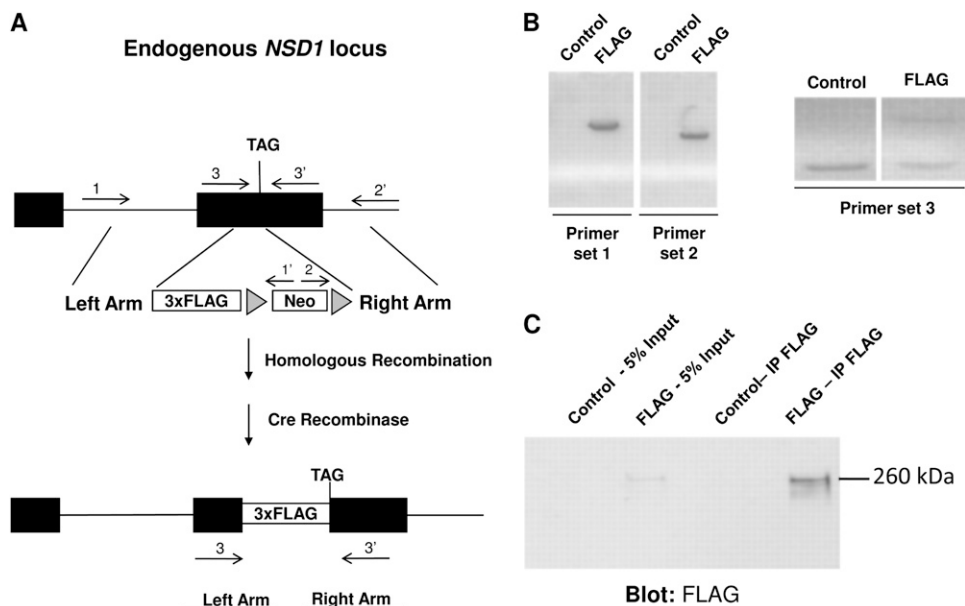


Fig. S1. Generation of an NSD1-FLAG line in HCT116 cells. Homologous recombination was used to generate HCT116 cell line expressing an epitope-tagged NSD1 protein from the endogenous chromosomal locus. (A) Diagram representing the method used to introduce the 3xFLAG sequences at the C terminus of NSD1. A targeting vector with left and right homology arms (flanking a 3xFLAG-loxP-neo) was packaged into adenovirus and used to transduce HCT116 cells. After selection, the Neo gene was excised using Cre recombinase resulting in a FLAG-tagged NSD1 gene. (B) PCR screening for successful recombinant clones. Neo-resistant clones were screened for correct HR events using PCR primers flanking the left arm and neo gene (primer set 1) and the right arm and neo gene (primer set 2). This results in a 2.0-kb product for the correct left arm placement and 1.5-kb product for the right arm. Primer set 3 was used to identify the 3xFLAG-positive clones in which the Neo gene was excised by Cre recombinase. After retroviral delivery of Cre, the control nontagged NSD1 gene yields a 225-bp product, whereas the FLAG-tagged NSD1 gene yields a 500-bp product using primer set 3. (C) Expression of NSD1-FLAG in HCT116 cells. IP followed by Western blotting showing the FLAG-tagged NSD1 protein and its absence in the control (non-FLAG-tagged) HCT116 cells. Importantly, this band, which represents the short isoforms, was absent in the control (non-FLAG-tagged) HCT116 cells, indicating that the cross-reacting material at 300 kDa is conclusively derived from the endogenous NSD1 gene.

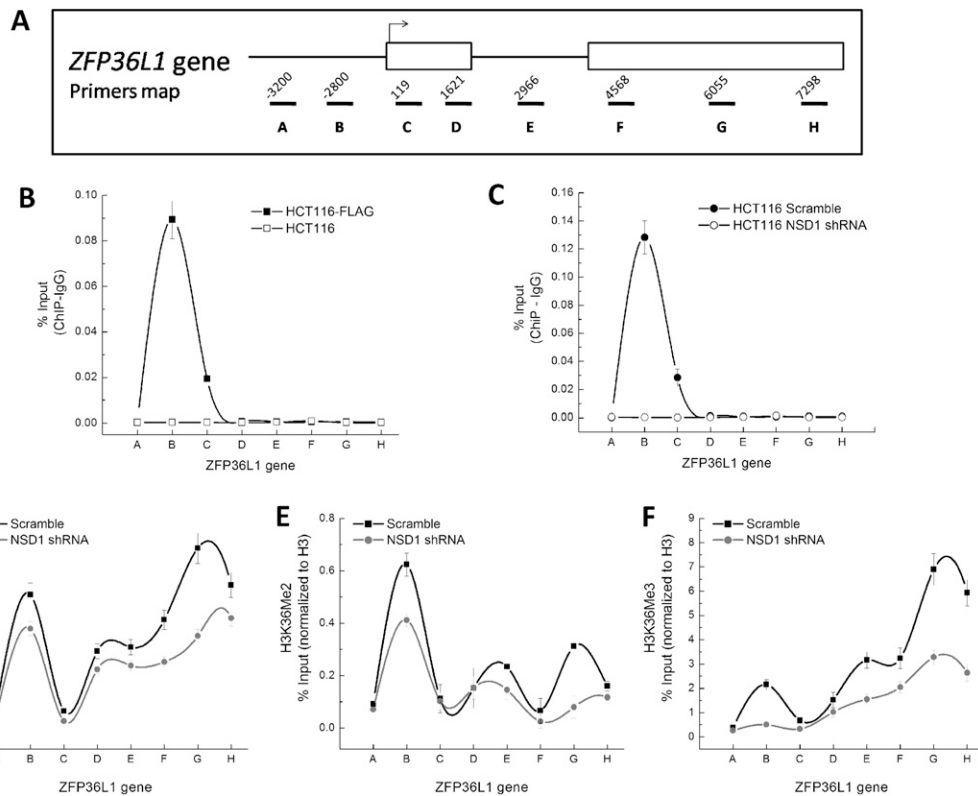


Fig. S2. (A) Diagram of *ZFP36L1* intron/exon gene structure (not drawn to scale) showing the location of amplicons used to determine the NSD1 binding profile at *ZFP36L1* gene. Numbers represent the first base of forward primer. The average sizes of amplicons are between 150 and 200 bp. Negative numbers indicate the region upstream +1 site (promoter region). Primer sequences are listed in Table S3. (B and C) NSD1 binding is concentrated upstream of the *ZFP36L1* promoter. HCT116 NSD1-FLAG cells were processed for ChIP using FLAG (B) or NSD1 (C) antibodies. All primer sets were validated by DNA sequencing and through their ability to amplify one band. Control cells (parental cells void of the FLAG-tag and cells depleted of NSD1 by shRNA) were used for ChIP with FLAG and NSD1 antibody, respectively, to show specificity of NSD1 binding. (D–F) H3K36 mono-, di-, and tri- H3K36 methylation profile at the *ZFP36L1* locus in the presence or absence of NSD1. The levels of mono (D), di (E), and tri (F) H3-K36 methylation were measured by ChIP using specific antibodies in HCT116 cells, followed by real-time PCR. Primers (A–L) were designed along *ZFP36L1* gene designed according to the diagram in A. ChIP-specific signal (% input) was calculated using IgG as control as specified in SI Materials and Methods. The % input values were normalized to total H3 (% input H3K36 Me/% input unmodified H3). Because the values were normalized by H3, values <1 may be expected. Error bars (B–F) represent SD from the mean ($n = 3$).

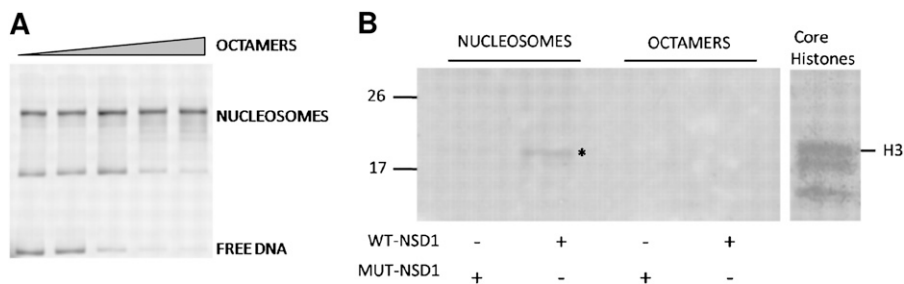


Fig. S3. NSD1 methylates nucleosomes on histone H3. (A) Generation of nucleosomes by a salt dialysis procedure. HeLa cell octamers were mixed with 200-bp DNA fragments to generate histone octamers. (B) Histone methyltransferase assay showing specificity of NSD1 for H3. Nucleosomes or octamers were used as a substrate. WT-NSD1 indicates an HA-tagged mouse NSD1 where residues 1–267 were removed. MUT-NSD1 was used as negative control and represents a catalytically inactive version of HA-mNSD1 (HA-mNSD1-mut) generated by a double-point mutation in the SET domain. Core histones were used as loading control. The asterisk represents H3.

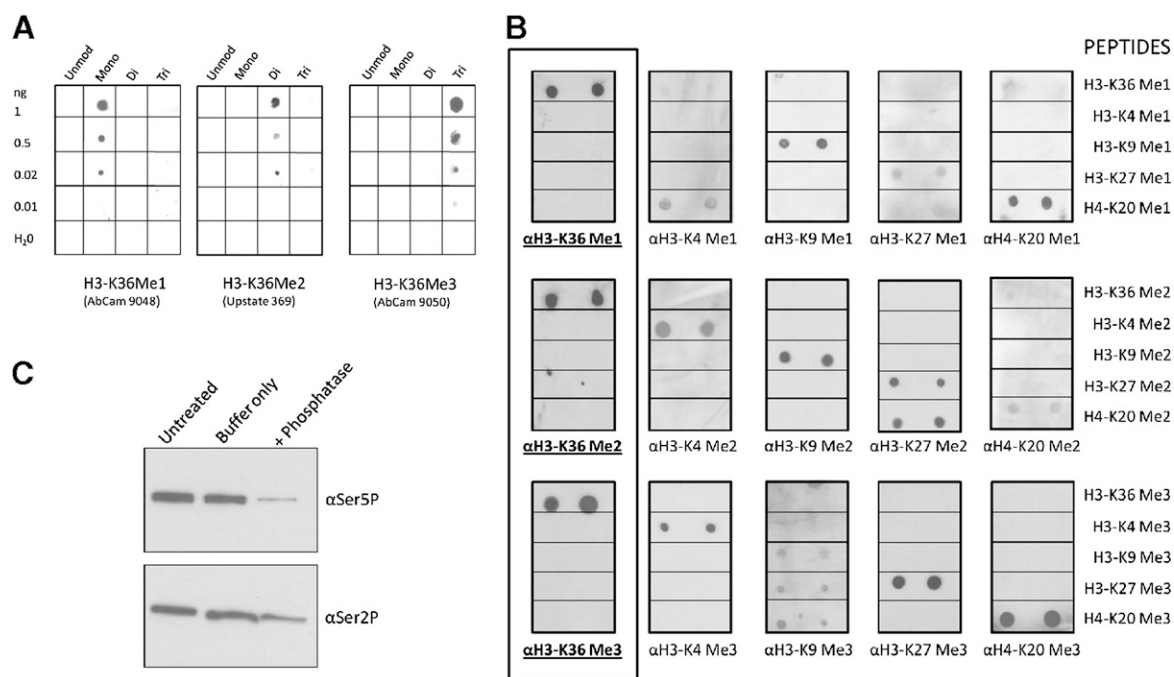


Fig. S4. Specificity of H3-K36Me1, Me2, and Me3 antibodies. (A) Dot blots with purified peptides (unmodified H3, H3-K36Me1, Me2, and Me3 from New England Peptide) were spotted on membranes and then blotted with the indicated primary and respective secondary antibodies. The labels on the left indicate the amount of purified peptide blotted on each membrane. (B) H3-K36 methylation specific antibodies fail to cross-react with various methylated lysines on peptides with sequences from histones H3 and H4. Purified methylated peptides (mono, di, and tri) at various positions on residues found in H3 and H4 were spotted (3 ng) in duplicate on nitrocellulose membranes and then blotted with specific antibodies (1:1,000 dilution), including H3-K36Me1, Me2, and Me3. Note that the H3-K36 methylation-specific antibodies do not cross-react with methylated lysines from other histone tails (boxed panels). All peptides were purchased from Epigentek. The antibodies used as positive controls were: H3-K4: Me1* (Epigentek 4031), Me2 (Epigentek 4032), Me3 (Active Motif 39159); H3-K9: Me1 (Epigentek 4034), Me2 (Active Motif 39239), Me3* (Abcam ab8898); H3-K27: Me1 (Upstate 07-488), Me2* (Epigentek 4038), Me3 (Epigentek 4039); H4-K20: Me1 (Epigentek 4046), Me2 (Epigentek 4047), and Me3 (Epigentek 4048). Asterisks represent antibodies that cross-react with nontarget antigens in dot blot experiments performed in our lab. (C) Phosphospecific antibodies against RNA Pol II (Bethyl Laboratories A310-190A) are specific for phosphorylated forms of RNA Pol II. Total HeLa cell lysate was incubated with buffer or alkaline phosphatase before fractionation on SDS/PAGE gels. After immunoblotting with phosphospecific antibodies directed against serine 5 and serine 2, the signal is significantly diminished in those samples treated with phosphatase.

Other Supporting Information Files

[Table S1 \(DOCX\)](#)

[Table S2 \(DOCX\)](#)

[Table S3 \(DOCX\)](#)